Research Square

Preprints are preliminary reports that have not undergone peer review.
They should not be considered conclusive, used to inform clinical practice,
or referenced by the media as validated information.

Physicochemical, colloidal, and thermogravimetric assessment of Brazilian Potiguar Basin crude oils with different API gravities

Bruno R. F. Nunes[1]
Federal University of Rio Grande do Norte
Italo A. S. Junior
Federal University of Rio Grande do Norte
Maria Paula N. M. R. Almeida
Federal University of Rio Grande do Norte
Stephanie S. Assunção
Federal University of Rio Grande do Norte
Wally T. Rocha
Federal University of Rio Grande do Norte
Ellen V. S. Ribeiro
Federal University of Rio Grande do Norte
Gisele S. S. Lima
Federal University of Rio Grande do Norte
Marcio D. S. Araujo
Federal University of Rio Grande do Norte
Jilliano B. Silva
Federal University of Rio Grande do Norte
Glauber J. T. Fernandes
CERNE – Center for Strategies in Natural Resources and Energy
Valter J. Fernandes
Federal University of Rio Grande do Norte
Antonio S. Araujo
antonio.araujo@ufrn.br

Federal University of Rio Grande do Norte

Research Article

Keywords: API gravity, crude oil, SARA, colloidal stability, thermogravimetry

Posted Date: November 17th, 2026

DOI: https://doi.org/10.21203/rs.3.rs-11246466/v1

License: This work is licensed under a Creative Commons Attribution 4.0 International License.
Read Full License

Additional Declarations: No competing interests reported.

Physicochemical, colloidal, and thermogravimetric assessment of Brazilian Potiguar Basin crude oils with different API gravities

Bruno R. F. Nunes[1], Italo A. S. Junior[2], Maria Paula N. M. R. Almeida[2], Stephanie S. Assunção[2], Wally T. Rocha[2], Ellen V. S. Ribeiro[2], Gisele S. S. Lima[2], Marcio D. S. Araujo[2], Jilliano B. Silva[2], Glauber J. T. Fernandes[3], Valter J. Fernandes Jr[2] and Antonio S. Araujo[1,2]*

[1]Graduate Program in Energy and Petroleum, Federal University of Rio Grande do Norte, 59078-970, Natal RN, Brazil

[2]Federal University of Rio Grande do Norte, Institute of Chemistry, 59078-970, Natal RN, Brazil

[3]CERNE – Center for Strategies in Natural Resources and Energy, 59064-390, Natal RN, Brazil

*Corresponding author: Antonio S. Araujo (antonio.araujo@ufrn.br)

Abstract

Thermogravimetry (TG) and derivative thermogravimetry (DTG) were used to correlate crude-oil composition and physicochemical properties with thermal mass-loss behavior and apparent kinetic and activation thermodynamic parameters. Three Brazilian Potiguar Basin oils, classified as light, medium, and heavy and spanning 15.4–32.7 °API, were analyzed under nitrogen at 10 °C min^{-1}. Decreasing API gravity was accompanied by higher viscosity, resin–asphaltene content, sulfur, nitrogen, and total acid number. These compositional changes coincided with a decreasing contribution from the volatilization region, accounting for approximately 86, 74, and 62 mass% of the light, medium, and heavy oils, respectively, and increasing final residues of 4, 7, and 10 mass%. Apparent volatilization activation energies increased from 65.1 to 69.9 and 80.6 kJ mol^{-1}, with corresponding activation enthalpies of 60.9, 65.6, and 75.5 kJ mol^{-1}, consistent with progressively greater resistance to molecular release. Cracking activation energies remained within 97.7–100.5 kJ mol^{-1}, indicating comparable effective barriers despite differences in composition and residue yield. Negative apparent activation entropies and positive activation Gibbs energies characterized the derived activation parameters, without establishing overall process spontaneity or calorimetric reaction enthalpies. The saturate-rich light oil exhibited the highest colloidal instability indices, demonstrating that dispersion stability and thermal resistance describe distinct properties. Integrated TG/DTG and compositional analysis differentiated volatilization-dominated light oil from the greater cracking contribution and residue formation of heavy oil, supporting preliminary feedstock assessment.

Keywords: API gravity; crude oil; SARA; colloidal stability; thermogravimetry

1. INTRODUCTION

Crude-oil value and processability are controlled not only by density but by the molecular distribution among saturates, aromatics, resins, and asphaltenes (SARA), together with heteroatoms and acidic species. API gravity remains the most widely used commercial descriptor, yet oils having similar gravity can differ in flow behavior, fouling tendency, hydrogen demand, corrosion risk, and product yield. An integrated characterization is therefore more useful than classification by a single property [1, 2].

The heavy end of petroleum behaves as a polydisperse colloidal system. Aromatics and resins contribute solvency and steric stabilization, whereas paraffinic saturates reduce asphaltene solubility. Changes in pressure, temperature, or composition can disturb this balance and promote aggregation and deposition. Recent thermal-modeling studies likewise identify temperature, API gravity, resins, and asphaltenes as influential predictors of the residual mass generated during crude-oil pyrolysis and oxidation [3, 4].

Thermogravimetry (TG) provides a compact thermal fingerprint of crude oil. Under inert gas, low- and intermediate-boiling constituents are removed predominantly by evaporation and distillation, whereas higher-temperature mass loss increasingly reflects bond scission, hydrogen transfer, condensation, and coke formation. Derivative thermogravimetry (DTG) helps resolve overlapping events and supplies characteristic temperatures for comparative screening. For Brazilian heavy oils and atmospheric residues, Araujo and collaborators demonstrated that TG could distinguish distillation and cracking domains, quantify catalytic shifts, and follow activation energy across conversion when multiple heating rates are used [5, 6, 7, 8]. Because petroleum degradation is multistep, kinetic quantities remain method-dependent; robust kinetic

analysis requires several heating rates and adherence to isoconversional recommendations [9].

This work compares light, medium, and heavy crude oils from the Potiguar Basin, from Rio Grande do Norte State, Northeastern Brazil. The objective was to connect API gravity, viscosity, SARA composition, sulfur, nitrogen, acidity, colloidal indices with the TG/DTG event distribution, and its kinetic and thermodynamic parameters. Unlike studies centered on a single residue, the present contribution uses the same analytical framework across three crude-oil classes to relate feed composition to flow assurance, distillability, cracking burden, and carbonaceous residue. The kinetic quantities are intentionally delimited as single-rate screening estimates, thereby separating defensible comparative interpretation from model-independent kinetic claims.

2. MATERIALS AND METHODS

2.1. Crude-oil samples

Three representative crude oils from the Potiguar Basin (Rio Grande do Norte, Brazil) were homogenized before analysis and designated PET-Light, PET-Medium, and PET-Heavy. Their measured API gravities were 32.7, 25.2, and 15.4°, respectively. Results are reported on as-received samples.

2.2. Physicochemical characterization

Relative density and API gravity were determined using standardized petroleum procedures consistent with ASTM D5002 [10]. Kinematic viscosity was measured at 20, 30, and 50 °C according to ASTM D445 [11]. SARA fractions were determined by adsorption chromatographic separation; asphaltenes corresponded to the n-heptane-

insoluble fraction. Total sulfur was measured by energy-dispersive X-ray fluorescence (ASTM D4294 [12]), total nitrogen by instrumental combustion analysis (ASTM D5291 [13]), and total acid number (TAN) by potentiometric titration with alcoholic KOH (ASTM D664 [14]). The analytical work was conducted at the Laboratory of Fuels and Lubricants – Federal University of Rio Grande do Norte, under its ISO/IEC 17025 quality system.

2.3. Colloidal indices

The colloidal instability index (CII) was calculated from mass fractions as follows:

$$CII = \frac{Saturates + Aphaltenes}{Aromatics + Resins} \quad (1)$$

A weighted colloidal stability index (CSI) was also calculated using dielectric weighting factors assigned to the four SARA families:

$$CSI = \frac{(\varepsilon^{asf})(Asphaltenes) + (\varepsilon^{sat})(Saturates)}{(\varepsilon^{res})(Resins) + (\varepsilon^{arom})(Aromatics)} \quad (2)$$

The factors used in the source dataset were 1.92, 2.38, 4.70, and 5.50 for saturates, aromatics, resins, and dispersed asphaltenes, respectively. CII > 0.90 and CSI > 0.95 were used as screening thresholds for potential colloidal instability. These indices are compositional indicators rather than direct precipitation tests.

2.4. Thermogravimetric analysis and apparent kinetic screening

Approximately 10–12 mg of homogenized oil was placed in a platinum pan and heated from ambient temperature to the upper experimental range under nitrogen flowing at approximately 50 mL min^{-1}. TG/DTG measurements were performed using TA Instruments equipment, model SDT 600, using alumina crucible. The linear heating rate was 10 °C min^{-1}. TG and DTG curves were used to identify the initial (T_i), peak-rate (T_{max}), and final (T_f) temperatures of the main mass-loss regions. Conversion was defined by $\alpha = (m_0 - mT)/(m_0 - m_f)$, where mT is the mass at a given temperature T.

Apparent activation energies were estimated from T_{max} using a simplified Arrhenius/Kissinger-type expression with an assumed pre-exponential factor $A = 1.0 \times 10^5$ s^{-1}. Activation enthalpy, entropy, and Gibbs energy were calculated from transition-state relationships. Since only one heating rate was available, these values are reported strictly as comparative screening estimates, not as validated Kissinger or isoconversional kinetic constants. Thus, kinetic validation of the present oils requires are consistent with ICTAC recommendations [9].

3. RESULTS AND DISCUSSION

3.1. Density and temperature-dependent viscosity

Density increased monotonically as API gravity decreased (Table 1). The most operationally important contrast was rheological: at 20 °C PET-Heavy was much more viscous than PET-Light. It was verified that heating to 50 °C reduced viscosity by about 70% for PET-Light, 72% for PET-Medium, and 94% for PET-Heavy, yet the heavy oil remained more than two orders of magnitude more viscous. The particularly strong thermal response of PET-Heavy is consistent with disruption of reversible associations

among aromatic and polar high-molar-mass species, while its high residual viscosity indicates persistent aggregate interactions.

Table 1. Density, API gravity, and kinematic viscosity of the crude oils.

Property	PET-Light	PET-Medium	PET-Heavy
API gravity (°API)	32.7	25.2	15.4
Relative density (20/4 °C)	0.8579	0.8996	0.9592
Viscosity at 20 °C ($mm^2\ s^{-1}$)	29.46	64.79	15,470
Viscosity at 30 °C ($mm^2\ s^{-1}$)	17.74	40.09	4,963
Viscosity at 50 °C ($mm^2\ s^{-1}$)	8.808	18.35	907.3

Figure 1 demonstrates the combined influence of temperature and API gravity on crude-oil viscosity. Viscosity decreases markedly with increasing temperature for all samples, confirming that heating enhances molecular mobility and reduces intermolecular interactions among petroleum constituents.

The heavy oil (15.4 °API) exhibits the strongest temperature dependence, decreasing from 15,470 $mm^2\ s^{-1}$ at 20 °C to 907.3 $mm^2\ s^{-1}$ at 50 °C, approximately 94% reduction. Nevertheless, it remains substantially more viscous than the other oils because of its higher content of resins, asphaltenes, and condensed aromatic structures. The medium oil (25.2 °API) decreases from 64.79 to 18.35 $mm^2\ s^{-1}$, while the light oil (32.7 °API) decreases from 29.46 to 8.808 $mm^2\ s^{-1}$ over the same temperature interval. Thus,

viscosity increases sharply as API gravity decreases, indicating greater molecular complexity and stronger associative interactions in heavier oils.

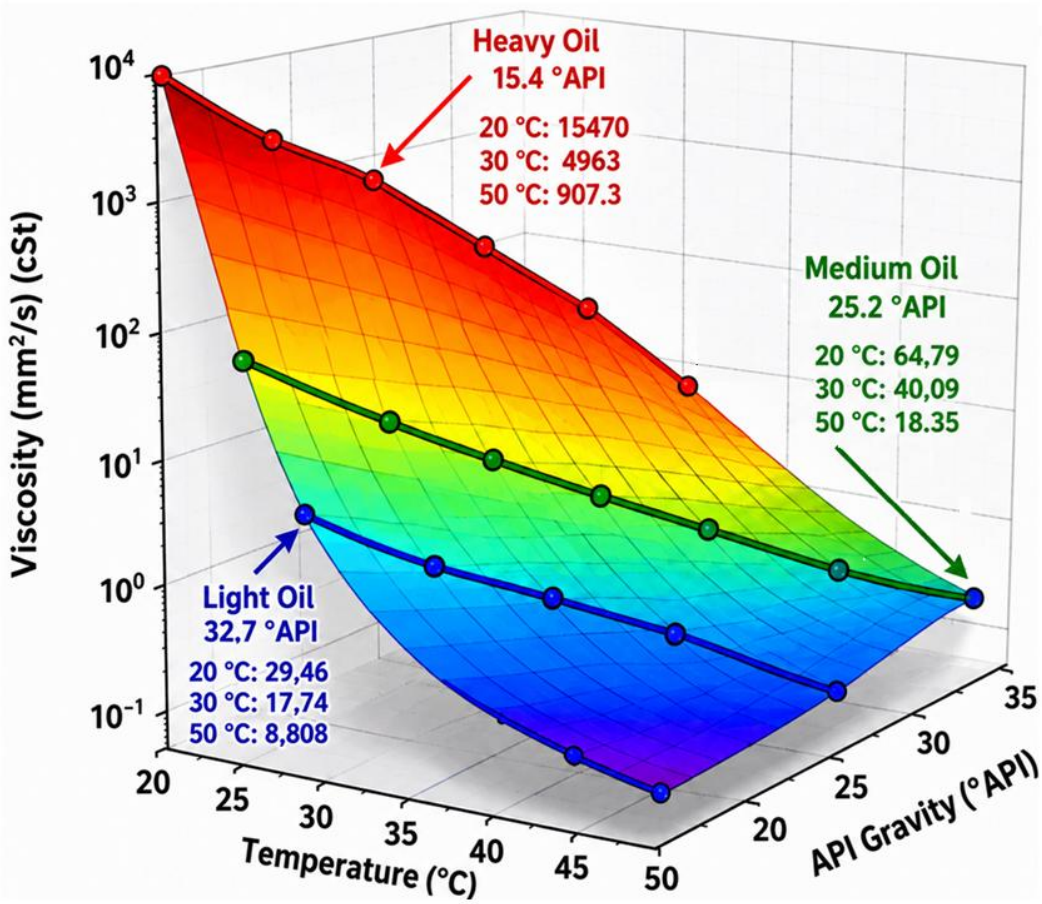


Figure 1. Degree API and temperature dependence of kinematic viscosity.

The 3D graphic (Figure 1) illustrates the combined influence of temperature and API gravity on the kinematic viscosity of the three crude oils. Based on the annotated measurements, viscosity decreases with increasing temperature for every sample, while the heavy oil consistently exhibits the greatest resistance to flow. At 20 °C, PET-Heavy (15.4 °API) has a viscosity of 15,470 $mm^2\ s^{-1}$, compared with 64.79 $mm^2\ s^{-1}$ for PET-Medium (25.2 °API) and 29.46 $mm^2\ s^{-1}$ for PET-Light (32.7 °API). The heavy oil is

therefore approximately 525 times more viscous than the light oil, demonstrating that the viscosity contrast is substantially greater than the difference in API gravity alone might suggest. Heating from 20 to 50 °C reduces viscosity by approximately 70.1% for PET-Light, 71.7% for PET-Medium, and 94.1% for PET-Heavy. The particularly strong response of the heavy oil is consistent with increased molecular mobility and weakening of intermolecular associations within its complex liquid matrix. Where supported by compositional measurements, aromatic and polar resin–asphaltene structures provide a plausible explanation for its high initial viscosity. However, viscosity depends on the molecular characteristics and interactions of these fractions as well as their concentrations; API gravity and bulk SARA composition cannot uniquely determine rheological behavior.

Despite its substantial thermal response, PET-Heavy retains a viscosity of 907.3 $mm^2\ s^{-1}$ at 50 °C, approximately 103 times that of PET-Light and 49 times that of PET-Medium. Heating therefore improves heavy-oil flowability markedly but does not eliminate the viscosity differences among the samples. These results support temperature control as an important measure for handling, pumping, and feed conditioning, although selecting an operating temperature requires consideration of hydraulic requirements and heating costs. The observed decrease over 20–50 °C should be interpreted primarily as a physical rheological response rather than evidence of thermal cracking. Likewise, the curved surface provides a visual interpolation among the measurements, not a validated predictive relationship for all crude oils. The principal conclusion is that the heavy oil gains the greatest relative benefit from heating while retaining the largest absolute flow resistance.

Overall, the surface highlights a nonlinear relationship among viscosity, temperature, and API gravity. Heating is particularly effective for improving heavy-oil

flowability, although it does not eliminate the pronounced viscosity differences associated with crude-oil composition. These results are directly relevant to pumping, pipeline transport, storage, blending, and refinery feed conditioning.

3.2. SARA distribution, heteroatoms, and acidity

The decline in API gravity was accompanied by depletion of saturates and enrichment in resins and asphaltenes (Table 2).

Table 2. SARA composition, heteroatoms, and total acid number.

Property	PET-Light	PET-Medium	PET-Heavy
Saturates (wt%)	72.1	48.3	41.2
Aromatics (wt%)	16.0	31.0	26.3
Resins (wt%)	11.1	18.8	28.7
Asphaltenes (wt%)	0.85	1.91	3.84
Sulfur (wt%)	0.23	0.57	0.77
Nitrogen (wt%)	0.12	0.35	0.40
TAN (mg KOH g^{-1})	0.08	0.25	1.60

The Table 2 reveals a pronounced compositional shift from PET-Light to PET-Heavy, characterized by depletion of saturates and enrichment in polar heavy fractions, heteroatoms, and titratable acidity. Saturates decrease from 72.1 to 41.2 mass%, while resins increase from 11.1 to 28.7 mass% and asphaltenes from 0.85 to 3.84 mass%. The combined resin–asphaltene fraction consequently rises from 11.95 to 32.54 mass%,

approximately a 2.7-fold increase. This redistribution provides a chemical basis for the higher viscosity, reduced volatility, and greater residue-forming potential of the heavy oil. Nevertheless, SARA fractions are operationally defined groups, and their concentrations alone do not establish molecular structures or individual reaction mechanisms.

PET-Light is dominated by saturated hydrocarbons and contains comparatively little resin and asphaltene material. This composition is consistent with its lower viscosity and greater contribution from physical volatilization during heating. However, the saturate fraction includes hydrocarbons spanning a broad molecular-size range; its abundance cannot be directly equated with gasoline or diesel yield. The relatively low aromatic content of 16.0 mass% also implies a less favorable solvent environment for asphaltenes than in the other samples. Consequently, low asphaltene concentration does not guarantee colloidal stability, particularly when the oil is blended with additional paraffinic streams.

PET-Medium exhibits the highest aromatic fraction, 31.0 mass%, compared with 16.0 mass% for PET-Light and 26.3 mass% for PET-Heavy. Aromatic content therefore follows a nonmonotonic trend, demonstrating that the compositional progression cannot be represented simply as a uniform increase in every nonsaturate fraction. Its combination of aromatics and resins can favor asphaltene dispersion, while the increased heavy-fraction content supports greater overlap between volatilization and decomposition. PET-Medium thus represents a distinct compositional balance rather than merely an average of the light and heavy oils.

PET-Heavy is particularly distinguished by its resin enrichment. Although its asphaltene concentration is approximately 4.5 times that of PET-Light, resins constitute the larger share of its polar heavy fraction. Its high viscosity should therefore be

interpreted through the interactions of the entire liquid matrix, including molecular size, aromaticity, polarity, and association, rather than attributed exclusively to asphaltenes. During heating, cleavage of peripheral chains and susceptible linkages can release lighter fragments, while retained aromatic-rich material can undergo secondary condensation. This competition offers a plausible explanation for simultaneous volatile-product generation and carbonaceous residue accumulation, although product and residue analyses are needed to confirm it.

The heteroatom results reinforce the increasing processing burden. Sulfur rises from 0.23 to 0.77 mass% and nitrogen from 0.12 to 0.40 mass%, corresponding to approximately 3.3-fold increases in both cases. These concentrations indicate a larger heteroatom-removal requirement for PET-Heavy when producing fuels of comparable quality. However, total sulfur and nitrogen do not reveal chemical speciation, which strongly affects removal difficulty and catalytic behavior. Hydrogen consumption and catalyst inhibition therefore cannot be quantified from these totals alone.

The most pronounced relative change occurs in total acid number (TAN), which increases twentyfold, from 0.08 to 1.60 mg KOH g^{-1}. PET-Heavy consequently warrants closer assessment of acid-related corrosion during hot processing. TAN measures neutralizable acidity rather than the concentration of a specific naphthenic-acid family, and it cannot independently predict corrosion rate. Acid structure, sulfur species, temperature, flow conditions, and equipment metallurgy must also be considered. The medium oil contained the largest aromatic fraction (31.0 wt%), whereas the heavy oil contained markedly more resins. This distinction matters because aromatics provide asphaltene solvency while resins can adsorb at aggregate surfaces. Consequently, API gravity or asphaltene content alone cannot fully predict colloidal behavior.

Taken together, the results distinguish a saturate-rich light feed, an aromatic-rich medium feed, and a resin-rich heavy feed with the greatest heteroatom and acidity burden. This integrated characterization supports differentiated handling and upgrading strategies and explains why API gravity alone is insufficient for feedstock selection. The observed trends are comparative findings for these three samples; without replicate measurements and uncertainty estimates, they should not be treated as universal relationships.

3.3. Colloidal screening

As observed in Figure 2. PET-Light yielded the highest CSI (1.587) and CII (2.69), despite containing only 0.85 wt% asphaltenes.

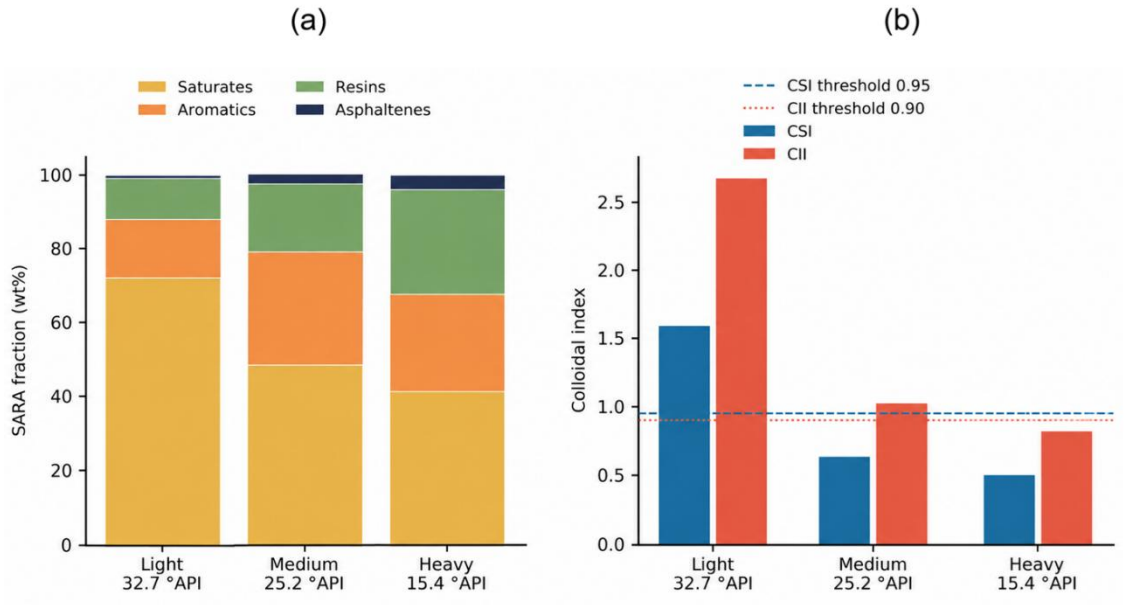


Figure 2. (a) SARA composition and (b) weighted colloidal stability index (CSI) and colloidal instability index (CII). Dashed lines indicate the thresholds in this work.

This apparently counterintuitive result follows from its high saturates-to-aromatics-plus-resins balance: abundant saturates have low solvency for asphaltenes. PET-Medium was marginal by CII (1.01) but below the CSI threshold (0.637), while

PET-Heavy gave CII = 0.82 and CSI = 0.508. Thus, the heavier oil was compositionally buffered by its high resin content under the index definitions used. The result should not be interpreted as proof that PET-Heavy cannot deposit asphaltenes; temperature, pressure, dilution, blending, and shear can shift the equilibrium. Direct onset or compatibility measurements would be required for operational qualification.

In Figure (a), decreasing API gravity is accompanied by a reduction in saturates—from approximately 72 wt% in the light oil to 41 wt% in the heavy oil—and progressive enrichment in resins and asphaltenes. The aromatic fraction is highest in the medium oil. This compositional evolution reflects the increasing molecular complexity, polarity, viscosity, and carbon-residue potential of heavier crude oils. Figure (b) shows that the light oil exceeds both instability thresholds, with CSI ≈ 1.59 and CII ≈ 2.69. Despite its low asphaltene content, its high proportion of saturates provides limited solvency for asphaltenes. The medium oil is below the CSI threshold but slightly above the CII limit, indicating borderline behavior. The heavy oil remains below both thresholds because its high resin content helps stabilize asphaltene aggregates. Thus, colloidal stability depends on the balance among all SARA fractions rather than solely on the absolute asphaltene concentration.

3.4. TG/DTG event distribution

The TG and DTG profiles separated the samples according to volatility and heavy-end content, as viewed in Figures 3 and 4, respectively. PET-Light lost approximately 86 wt% before the higher-temperature cracking region, compared with 74 wt% for PET-Medium and 62 wt% for PET-Heavy. Conversely, cracking-region mass loss increased from about 10 to 28 wt%, and final residue increased from 4 to 10 wt% as API gravity declined, as given in Table 3.

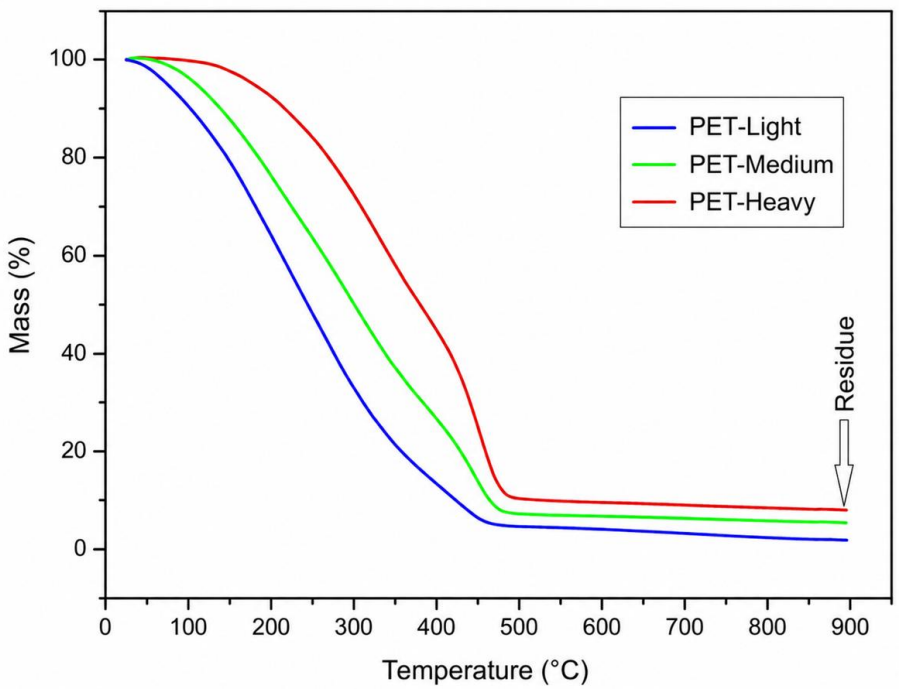


Figure 3. TG curves of the light, medium, and heavy crude oils under nitrogen at 10 °C min^{-1}.

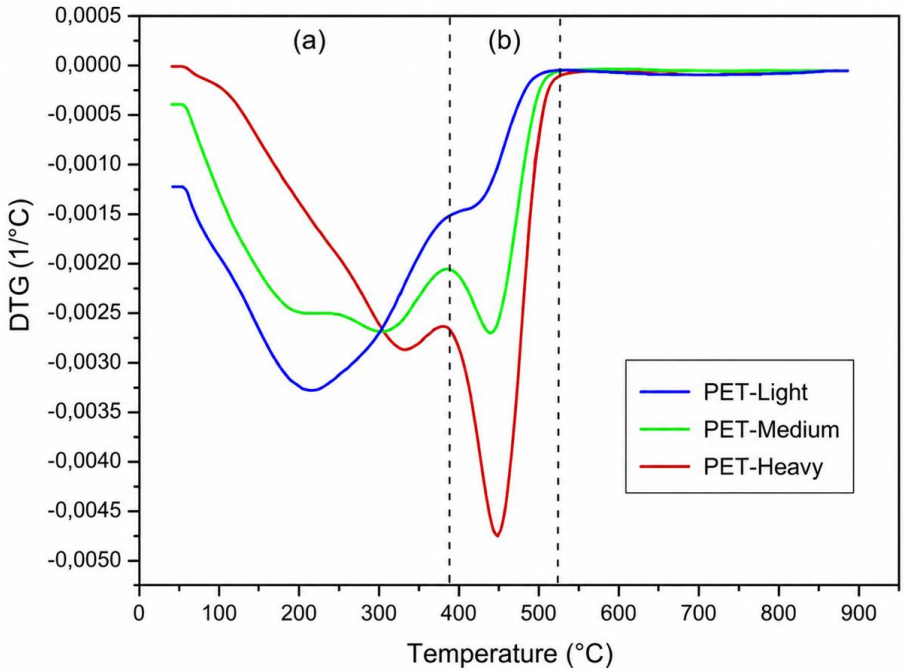


Figure 4. DTG curves showing (a) volatilization/distillation and (b) higher-temperature cracking regions.

Table 3. Characteristic TG/DTG temperatures and approximate mass distribution.

Sample	Event	T_i (°C)	T_{max} (°C)	T_f (°C)	Mass (wt%)
PET-Light	Volatilization	45	220	380	86
	Cracking	380	455	520	10
	Final residue	—	—	—	4
PET-Medium	Volatilization	50	255	385	74
	Cracking	385	470	527	19
	Final residue	—	—	—	7
PET-Heavy	Volatilization	55	330	388	62
	Cracking	388	450	550	28
	Final residue	—	—	—	10

The volatilization peak shifted from 220 °C for PET-Light to 330 °C for PET-Heavy, directly reflecting the progressive replacement of lower-boiling constituents by less volatile polar and aromatic material. The cracking maxima did not follow the same monotonic order (455, 470, and 450 °C). Crude-oil cracking comprises parallel volatilization, scission, hydrogen-transfer, condensation, and coke-forming reactions; T_{max} therefore represents a composite rate maximum rather than a unique molecular reaction. The larger cracking-stage mass fraction and residue of PET-Heavy are more robust indicators of conversion burden than the small difference in peak temperature. This interpretation agrees with Araujo and collaborators, who observed composition dependent shifts during TG of Brazilian heavy crude oil and atmospheric residue [5, 7,

8], and with large-data modeling that identifies temperature, API gravity, resins, and asphaltenes as major predictors of residual mass [3, 4].

The TG curves show that thermal behavior is strongly influenced by API gravity. PET-Light loses mass at lower temperatures and retains only about 4% residue, reflecting its higher proportion of volatile saturated hydrocarbons. PET-Medium presents intermediate behavior, whereas PET-Heavy decomposes at higher temperatures and leaves approximately 10% residue because of its greater content of resins, asphaltenes, and condensed aromatic structures.

The DTG curves distinguish between two principal thermal regions. Region (a), extending approximately to 380–400 °C, is dominated by volatilization and distillation of light and intermediate fractions. PET-Light exhibits its principal mass-loss rate at lower temperatures, while the corresponding events shift toward higher temperatures as the oil becomes heavier. Region (b), approximately 400–520 °C, is associated mainly with thermal cracking of high-molecular-weight fractions. The intense PET-Heavy peak near 450 °C indicates substantial decomposition of resins and asphaltenes. Together, TG and DTG demonstrate that decreasing API gravity reduces volatility, shifts thermal events toward higher temperatures, increases the contribution of thermal cracking, and produces more carbonaceous residue.

3.5. Apparent kinetic and thermodynamic parameters

The apparent volatilization activation energy increased from 65.1 to 80.6 kJ mol^{-1} with decreasing API gravity, consistent with progressively less volatile material and stronger intermolecular association. Cracking values clustered near 98–101 kJ mol^{-1}, supporting a common energetic scale for the composite high-temperature event.

The numerical values are sensitive to the assumed A value and peak assignment. The true Kissinger slope requires T_{max} values measured and isoconversional methods require temperatures at fixed conversion across several heating programs. Accordingly, Table 4 is suitable for internal comparison only.

Table 4. Apparent single-rate kinetic and thermodynamic screening parameters.

Sample	Process	E_a (kJ mol^{-1})	ΔH (kJ mol^{-1})	ΔS (J mol^{-1} K^{-1})	ΔG (kJ mol^{-1})
PET-Light	Volatilization	65.1	60.9	−161.7	140.7
	Cracking	98.4	92.3	−164.9	212.4
PET-Medium	Volatilization	69.9	65.6	−162.3	151.3
	Cracking	100.5	94.4	−165.1	217.1
PET-Heavy	Volatilization	80.6	75.5	−163.4	174.1
	Cracking	97.7	91.7	−164.9	210.9

The thermal conversion of PET-Light, PET-Medium, and PET-Heavy under nitrogen is interpreted as overlapping molecular volatilization, radical decomposition, and secondary condensation. These pathways are proposed on the basis of the apparent activation parameters and established petroleum chemistry. Recent combined TG and pyrolysis work on crude oils supports the use of product characterization alongside kinetic analysis to distinguish overlapping thermal processes [15].

At lower temperatures, mass loss can arise from release of intact hydrocarbons without covalent-bond cleavage:

$$HC(liquid) \rightarrow HC(vapor)$$

Here, HC denotes a petroleum constituent, and the arrow represents physical transfer rather than an elementary chemical reaction. Release depends on volatility, intermolecular interactions, and transport through the evolving liquid matrix. Temperature-resolved pyrolysis research demonstrates that the energy associated with molecular release can include both matrix interactions and volatilization, whereas higher-temperature release can additionally involve covalent-bond breaking [16]. This distinction supports interpreting the present volatilization energies as effective release parameters rather than individual bond-dissociation energies.

PET-Light has the lowest apparent volatilization activation energy, 65.1 kJ mol^{-1}, consistent with preferential release of readily volatile constituents. Its remaining, less volatile fraction can subsequently undergo cracking. PET-Medium exhibits an intermediate release barrier of 69.9 kJ mol^{-1} and is interpreted as having greater overlap between evaporation and decomposition. PET-Heavy exhibits the largest barrier, 80.6 kJ mol^{-1}, approximately 24% above PET-Light. This ordering is consistent with reduced volatility and stronger retention in the heavy-oil matrix. Resin–asphaltene association is a plausible contributing factor were supported by the measured SARA composition, but the activation parameters alone do not identify the interactions responsible.

At higher temperatures, a plausible initiation step is homolytic cleavage of susceptible C–C linkages in alkyl chains, substituents, and bridges, producing carbon-centered radicals:

$$R\text{-}R' \rightarrow R\cdot + R'\cdot$$

The radicals can propagate decomposition through hydrogen abstraction and β-scission:

$$R\cdot + R'\text{-}H \rightarrow R\text{-}H + R'\cdot$$

$$R_1\text{-}CH_2\text{-}CH_2\text{-}CH_2\bullet \rightarrow R_1\text{-}CH_2\bullet + CH_2{=}CH_2$$

These schematic reactions conserve atoms and illustrate possible pathways rather than identified intermediates. R, R, and R_1 represent organic groups; • denotes an unpaired electron. Hydrogen abstraction transfers radical reactivity, while β-scission generates smaller radical fragments and an alkene. Radical recombination and disproportionation provide competing termination routes. A recent experimental study of isolated asphaltene cracking describes free-radical transformations and the competition between fragmentation and formation of heavier products [17].

For PET-Light, the proposed cracking contribution is associated with less volatile material retained after evaporation, including longer chains and alkyl substituents. PET-Medium is expected to combine these pathways with a larger contribution from retained aromatic and polar constituents, subject to confirmation by composition and product analysis. For PET-Heavy, cleavage of peripheral chains and interunit linkages can release smaller products while aromatic-rich structures remain in the condensed phase. This interpretation does not require wholesale destruction of condensed aromatic cores.

The apparent cracking energies, 98.4, 100.5, and 97.7 kJ mol^{-1} for PET-Light, PET-Medium, and PET-Heavy, respectively, span only 2.8 kJ mol^{-1}. Without uncertainty estimates, their ordering should not be taken as evidence of distinct intrinsic reactivities or a common rate-determining elementary step. Fragmentation competes with recombination, cyclization, dehydrogenation, and condensation of retained fragments. These reactions can progressively produce a less volatile carbon-rich residue:

$$\text{Retained heavy fragments} \rightarrow \text{Carbonaceous residue} + \text{volatile products}$$

This expression represents an overall reaction network rather than a balanced molecular equation. Experimental kinetic modeling of heavy-oil thermal cracking has explicitly treated SARA fractions together with gaseous products and coke, illustrating the need to account for several product pools [18]. The relative extent of residue formation depends on composition, temperature, residence time, hydrogen transfer, and vapor removal. Accordingly, a lower apparent cracking barrier for PET-Heavy does not imply a lower heat requirement or a lower tendency to generate residue. The latter interpretation must be supported by measured residue yields and characterization.

The proposed distinction among the oils therefore concerns the relative contributions of pathways: preferential intact-molecule release in PET-Light; increased overlap of release and decomposition in PET-Medium; and stronger competition between fragmentation and residue-forming reactions in PET-Heavy. This is a working mechanistic interpretation, not a mechanism established by the table.

The activation enthalpies derived from kinetic expressions must remain distinguished from measured heats of vaporization or decomposition. These complementary measurements are necessary to connect mass loss and thermal effects without assigning an unsupported molecular mechanism.

Figures 5 (a) and (b) show a clear relationship between crude-oil composition, API gravity, apparent activation energy, and residue formation. As API gravity decreases from 32.7° for the light oil to 15.4° for the heavy oil, the apparent activation energy of volatilization rises from approximately 65 to 81 kJ mol^{-1}. This increase reflects the lower volatility and stronger intermolecular association of resin- and asphaltene-rich fractions. Thermal-cracking energies remain comparatively similar, around 98–101 kJ mol^{-1}, indicating a comparable energetic barrier for decomposition of the heavy fractions. The second graph confirms that the final residue increases with the combined resin and

asphaltene content. The light, medium, and heavy oils generate approximately 4, 7, and 10 wt% residue, respectively. Thus, heavier oils require more energy during volatilization and exhibit greater coke-forming potential because of their higher concentration of thermally stable, condensed aromatic structures.

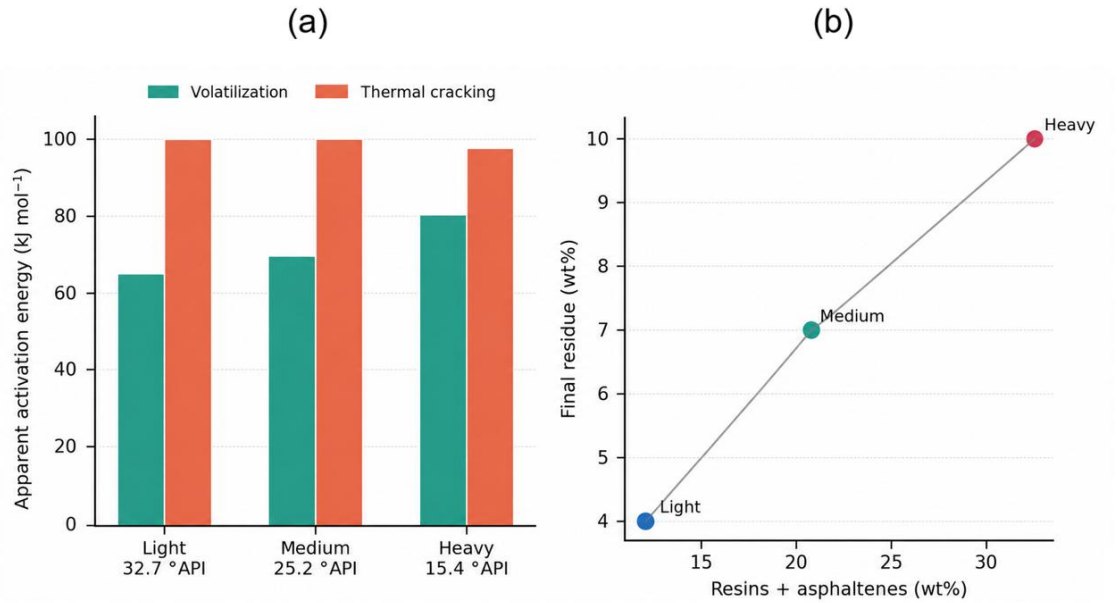


Figure 5. (a) Apparent activation-energy estimates for the two thermal regions and (b) relationship between polar heavy fractions and final TG residue.

Positive ΔH values denote an endothermic barrier, while negative ΔS values arise partly from the assumed common pre-exponential factor and imply a more constrained apparent activated state. Positive ΔG values indicate a substantial activation barrier; they should not be described as the bulk process being thermodynamically "nonspontaneous," because activation free energy concerns rate rather than equilibrium spontaneity.

3.6. Processing implications

The integrated results define distinct handling and processing profiles. PET-Light offers high atmospheric-distillable mass but may be compositionally vulnerable to asphaltene destabilization when blended or diluted with paraffinic streams. PET-Medium combines intermediate viscosity with relatively high aromatic solvency and borderline CII. PET-Heavy requires heating or viscosity-reduction measures for transport, presents the highest acidity and heteroatom burden, and directs more feed to thermal or catalytic conversion with greater coke propensity. For Potiguar refinery residues, catalytic distillation has been shown to lower final distillation temperatures and redistribute products toward gasoline or diesel ranges, illustrating a practical valorization route for the heavy fraction identified here [19]. These trade-offs show why crude selection and blending should use SARA balance, acidity, and thermal residue together with API gravity.

4. CONCLUSIONS

Thermogravimetry coupled with compositional and physicochemical characterization distinguished the thermal behavior of the three Brazilian Potiguar Basin crude oils more effectively than API gravity alone. From PET-Light to PET-Heavy, enrichment in resin–asphaltene fractions from 11.95 to 32.54 mass% accompanied higher viscosity, heteroatom content, and acidity, together with a shift toward higher-temperature mass loss and greater residual mass. Heating from 20 to 50 °C reduced heavy-oil viscosity by approximately 94%, but its remaining flow resistance demonstrated that thermal conditioning does not eliminate composition-dependent handling constraints.

TG/DTG provided the clearest evidence of the changing balance between volatilization and decomposition. The volatilization-region mass loss decreased from 86 to 74 and 62 mass% for the light, medium, and heavy oils, respectively, while cracking-region mass loss increased from 10 to 19 and 28 mass% and final residue rose from 4 to 7 and 10 mass%. The volatilization peak shifted from 220 to 330 °C, whereas cracking peak temperatures followed a nonmonotonic sequence. Thus, the amount of material entering the higher-temperature region and the resulting residue differentiated the oils more clearly than cracking peak temperature alone.

Apparent volatilization activation energies increased from 65.1 to 80.6 kJ mol^{-1}, with corresponding activation enthalpies increasing from 60.9 to 75.5 kJ mol^{-1}, consistent with greater resistance to molecular release in the heavier oil. In contrast, cracking activation energies remained within 97.7–100.5 kJ mol^{-1} despite substantial differences in mass-loss partitioning. The derived activation entropies and Gibbs energies describe assumption-dependent activation parameters; they do not establish overall process spontaneity, calorimetric heat requirements, or a unique decomposition mechanism. Their use is therefore restricted to comparative screening because they were estimated from a single heating rate and an assumed pre-exponential factor.

Colloidal screening revealed a complementary distinction: the saturate-rich light oil exhibited the highest instability indices despite its low asphaltene concentration. Dispersion stability consequently cannot be inferred from oil heaviness or equated with resistance to volatilization. The main contribution of this study is an integrated framework linking feed composition to flow resistance, thermal mass-loss distribution, and residue formation. Within the three-oil dataset, this approach supports preliminary decisions on thermal conditioning, compatibility testing, and upgrading requirements.

Acknowledgments

The authors acknowledge the Federal University of Rio Grande do Norte, the Fuels and Lubricants Laboratory, and the Catalysis and Petrochemistry Laboratory for analytical infrastructure. The authors also acknowledge CNPq and ANP for support to petroleum research and human-resource development.

Disclosure statement

The authors declare no potential conflict of interest.

Funding

This work received institutional and research support from the National Council for Scientific and Technological Development (CNPq, Grant 407460/2025-0).

Author contributions

Bruno R. F. Nunes, Italo A. S. Junior, Maria Paula N. M. R. Almeida, Stephanie S. Assunção, Wally T. Rocha, Ellen V. S. Ribeiro, Gisele S. S. Lima: investigation and data curation. Marcio D. S. Araujo, Glauber J. T. Fernandes, Jilliano B. Silva: data curation and graphics. Valter J. Fernandes Jr.: supervision, methodology, review and editing. Antonio S. Araujo: conceptualization, supervision, project administration, interpretation, and review and editing.

REFERENCES

1. Speight JG. The chemistry and technology of petroleum. 5th ed. Boca Raton: CRC Press; 2014.
2. Mullins OC. The Modified Yen Model. Energy Fuels. 2010;24:2179-2207. https://doi.org/10.1021/ef900975e
3. Hadavimoghaddam F, Rozhenko A, Mohammadi MR, Mostajeran Gortani M, Pourafshary P, Hemmati-Sarapardeh A. Modeling crude oil pyrolysis process using advanced white-box and black-box machine learning techniques. Sci Rep. 2023;13:22649. https://doi.org/10.1038/s41598-023-49349-x
4. Mohammadi MR, Hosseini SMM, Amiri-Ramsheh B, Kar S, Abedi A, Hemmati-Sarapardeh A, Mohaddespour A. Modeling residue formation from crude oil oxidation using tree-based machine learning approaches. Sci Rep. 2025;15:26264. https://doi.org/10.1038/s41598-025-10012-2
5. Coriolano ACF, Oliveira AAA, Bandeira RAF, Fernandes VJ Jr., Araujo AS. Kinetic study of thermal and catalytic pyrolysis of Brazilian heavy crude oil over mesoporous Al-MCM-41 materials. J Therm Anal Calorim. 2015;119:2151-2157. https://doi.org/10.1007/s10973-015-4408-4
6. de Araújo LCLF, de Moura Dantas TC, de Morais Araújo AM, Gondim AD, Fernandes Júnior VJ, de Araújo AS. Kinetic study on the thermal degradation of heavy oil in presence of SBA-15 containing aluminum and cerium. Pet Sci Technol. 2017;35:1396-1402. https://doi.org/10.1080/10916466.2017.1334061
7. Aquino CB, Silva JMR, Oliveira MHR, Coriolano ACF, Delgado RCOB, Fernandes VJ Jr., Araujo AS. Thermogravimetry applied for catalytic degradation of

atmospheric residue of petroleum on mesoporous catalyst. J Therm Anal Calorim. 2019;136:2139-2144. https://doi.org/10.1007/s10973-018-7830-6

8. Souza MRO, Silva JMR, Araujo MDS, Almeida JS, Fernandes VJ, Coriolano ACF, Delgado RCOB, Araujo AS. Kinetic study of distillation and cracking of heavy oil on bimodal meso–macroporous materials of silica and aluminosilicate by thermogravimetry. J Therm Anal Calorim. 2022;147:3647-3658. https://doi.org/10.1007/s10973-021-10765-8

9. Vyazovkin S, Burnham AK, Favergeon L, Koga N, Moukhina E, Pérez-Maqueda LA, Sbirrazzuoli N. ICTAC Kinetics Committee recommendations for analysis of multi-step kinetics. Thermochim Acta. 2020;689:178597. https://doi.org/10.1016/j.tca.2020.178597

10. ASTM International. ASTM D5002-24: Standard test method for density, relative density, and API gravity of crude oils by digital density analyzer. West Conshohocken: ASTM International; 2024.

11. ASTM International. ASTM D445-24: Standard test method for kinematic viscosity of transparent and opaque liquids. West Conshohocken: ASTM International; 2024.

12. ASTM International. ASTM D4294-21: Standard test method for sulfur in petroleum and petroleum products by energy-dispersive X-ray fluorescence spectrometry. West Conshohocken: ASTM International; 2021.

13. ASTM International. ASTM D5291-21: Standard test methods for instrumental determination of carbon, hydrogen, and nitrogen in petroleum products and lubricants. West Conshohocken: ASTM International; 2021.

14. ASTM International. ASTM D664-24: Standard test method for acid number of petroleum products by potentiometric titration. West Conshohocken: ASTM International; 2024.

15. Ghorbannezhad P, Can Seyfeli R, Serkan Uzyol K, Ceylan S, Hussain Tahir M, Ali I. Kinetics of thermal decomposition of crude oils: Insights from principal component analysis and products characterization. Fuel. 2024;359:130520. https://doi.org/10.1016/j.fuel.2023.130520

16. Lu K, Xue J, Liu Z. Deciphering the binding strength of oil matrix through molecularly resolved release energy analysis using thermal slicing ramped pyrolysis GC-MS. Anal Bioanal Chem. 2025;417:6339-6352. https://doi.org/10.1007/s00216-025- 06110-9

17. Félix G, Tirado A, Varfolomeev MA, Lugo-Medina E, Soto-Robles CA, Ancheyta J. Study on the Isolated Asphaltene Thermal Cracking from an Unconventional Oil Using Diverse Estimating Arrhenius Parameter Approaches. Molecules. 2025;30:4468. https://doi.org/10.3390/molecules30224468

18. Zhao S, Tang X, Pu W, He M, Yang Y. Kinetic modeling for upgrading of heavy crude oil via thermal cracking in porous media: SARA fractions and gas compositions. Fuel. 2024;371:132087 https://doi.org/10.1016/j.fuel.2024.132087

19. Morais CGDP, Silva JB, Almeida JS, Oliveira RR, Araujo MDS, Fernandes GJT, Delgado RCOB, Coriolano ACF, Fernandes VJ Jr., Araujo AS. Catalytic Distillation of Atmospheric Residue of Petroleum over HY-MCM-41 Micro-Mesoporous Materials. Catalysts. 2023;13:296. https://doi.org/10.3390/catal13020296